EEET ECOLOGICAL ENGINEERING & ENVIRONMENTAL TECHNOLOGY

Ecological Engineering & Environmental Technology 2023, 24(1), 272–286
https://doi.org/10.12912/27197050/154937
ISSN 2719-7050, License CC-BY 4.0

Received: 2022.09.15
Accepted: 2022.10.20
Published: 2022.11.01

Monitoring Land Use and Land Cover Changes Using Remote Sensing Techniques and the Precipitation-Vegetation Indexes in Morocco

Fatiha Ait El Haj[1*], Latifa Ouadif[2], Ahmed Akhssas[2]

[1] L3GIE Laboratory, Mohammadia Engineering School, Mohammed V University in Rabat, Morocco
* Corresponding author's e-mail: aitelhaj@emi.ac.ma

ABSTRACT

The study of land use and land cover change (LULC) is essential for the development of strategies, monitoring and control of the ecosystem. The present study aims to describe the dynamics of land cover and land use, and specially the impact of certain climatic parameters on the distribution of vegetation and land cover. For this study, multi-temporal remote sensing data are used to monitor land cover changes in Morocco, using a set of Landsat images, including Landsat 7 (ETM+), Landsat 5 (TM), and Landsat 8 (OLI), captured during the period 2000–2020, those changes were determined by adopting the maximum likelihood (ML) classification method. The classification results show good accuracy values in the range of 90% (2000), 80% (2007), 82% (2010), 93% (2020). The LU/LC change detection showed a decrease of agricultural and forest areas in the order of 5% between the year 2000 and 2020, and an increase of bare soil of 5% to 6%, and a notable change in urban area from 97.31 ha (0.03%) in 2000 to 2988.2637 ha (0.82%) in 2020. The overall results obtained from LULC show that the vegetation cover of the study area has undergone major changes during the study period. In order to monitor the vegetation status, an analysis of the precipitation-vegetation interaction is essential. The normalized difference vegetation index (NDVI) was determined from 2000 to 2020, to identify vegetation categories and quantify the vegetation density in the Lakhdar sub-basin. The obtained NDVI was analyzed using climatic index SPI (Normalized Precipitation Index) based on rainfall data from five stations. The correlation study between NDVI and SPI indices shows a strong linear relation between these two indicators especially while using an annual index SPI12 however, the use of NDVI index based on remote sensing provides a significant result while assessing vegetation. The results of our study can be used for vegetation monitoring and sustainable management of the area, since it is one of the largest basins in the country.

Keywords: LULC, remote sensing, GIS, kappa, landsat, NDVI, SPI.

INTRODUCTION

The use of satellite images and data to assess and analyze changes in land use and land cover [Chowdhury et al., 2020; Congedo, 2020; Chavez, 1988], has become the most recognized and powerful technique to obtain more accurate information on land surface characteristics at different temporal and spatial scales. These images also allow the analysis of vegetation conditions and their response to climate change. In Morocco, several researches have been conducted to study land use using remote sensing data. [Barakat et al., 2018] used multispectral ASTER (Advanced Spaceborne Thermal Emission and Reflection Radiometer) and Sentinel-2A data acquired in 2001 and 2015, to monitor forest cover dynamics in the eastern area of Beni-Mellal province, the study was based on the supervised classification algorithm and NDVI combined in a GIS environment to quantify the extent of change in the density of forest stands, the result revealed an overall change in forest cover with an increase in the wooded area. [Gurgel et al., 2017] identified forest changes in argan forests (Morocco) using aerial photographs and satellite images between 1970 and 2007. Their study revealed a decrease in forest density of 44.5% during this period.

For our case study, Landsat5-TM, Landsat7-ETM+, Landsat8-OLI satellite images are used to

identify changes and map land cover, it consists of a set of images at different dates (from the year 2000 to 2020) taken at the same period of the year, to capture the conditions of the study area and improve the classification of changes over different periods.

In order to classify and analyze the changes LULC in the Morocco sub-basin, we performed the maximum likelihood method. This is the most efficient algorithm for supervised classification [Bonn & Rochon, 1993; Chatelain, 1996], which seeks to build a function called the likelihood function and to maximize its logarithm considering the unknown parameters. The coherence of the maps obtained was evaluated using the value of the Kappa coefficient. To measure and research how vegetation responds to climate change, meteorologists and climatologists from all over the world have developed a variety of drought indicators. Indicators that are simple to calculate and statistically significant. McKee, Doesken, and Kleist, three American scientists, developed the Standardized Precipitation Index (SPI) in 1993 [Mckee et al. 1995]. SPI is a powerful, flexible, and easy-to-calculate index, precipitation is actually the only required input parameter. Furthermore, it works just as well for evaluating dry periods and cycles as it does for assessing wet ones. Landsat satellites have particular characteristics in terms of spatial, spectral and temporal resolution. The choice of this type of satellite favors the study and analysis of surface reflectance. Among the monitoring indices of vegetation dynamics that is based on the monitoring of surface reflectance is the normalized difference vegetation index (NDVI) used to better characterize the spatial extent of drought events and to monitor the vegetation status [Congedo, 2020; Abebe et al. 2022; Jiang et al. 2022]. In summary, the objective of this study is to explore the changes of LU/LC of the sub-basin in Morocco and to monitor the vegetation status that is affected by precipitation inputs and drought status in the area. The results of this study could be useful for vegetation monitoring and sustainable management of the area as it is one of the largest basins in Morocco.

MATERIALS AND METHODS

Study area

The sub-basin of *Lakhdar* [AHT Group, 2016] belongs to the hydraulic system of *wadi Oum Er-Rbia Which* belongs to the mountain area of the province of Beni-Mellal and has an area of 3503 km^2. The *Lakhdar* sub-basin is located at the eastern end of the *Haouz Mejjate* basin, bounded to the south and south-east by the High Atlas mountains and to the west by the *Tassaout* sub-basin (Figure 1). The topography [AHT Group, 2016]

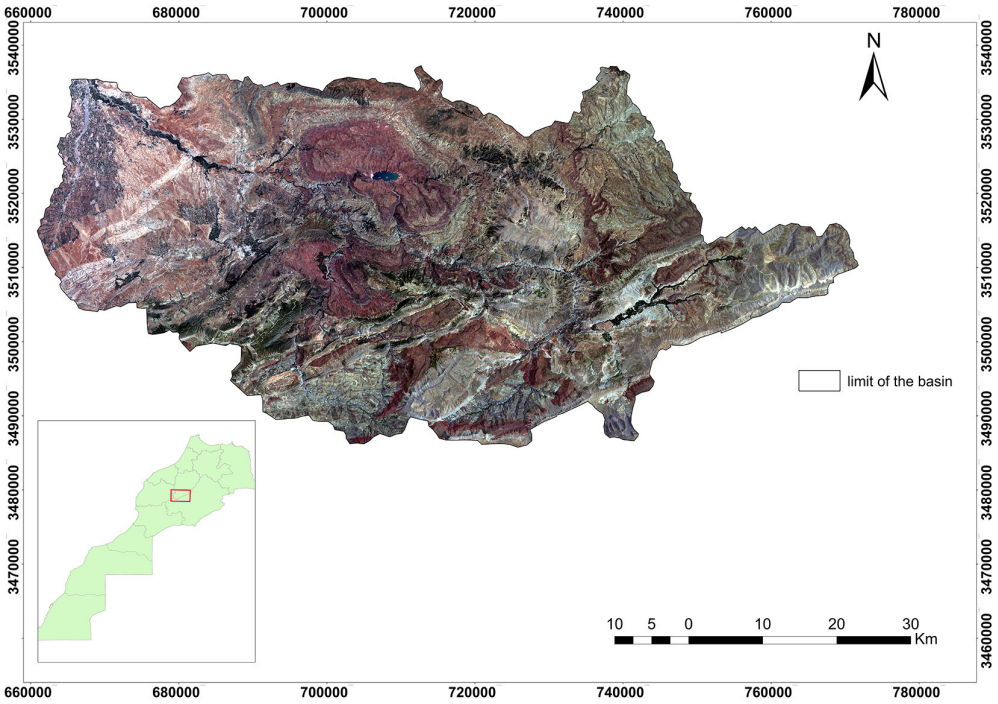

Figure 1. Location map of the Lakhdar sub-basin

of *Lakhdar* sub-basin is relatively rugged, and characterized by the variation in altitude between 488 m at the *Tensift wadi*, to 4017 m at the High Atlas.The *Lakhdar* sub-basin is drained [AHT Group, 2016] by the main watercourse (*Wadi Lakhdar*) which drains the western and south-western parts of the basin, its main tributary is *Wadi Bernat* which drains the northern and north-eastern parts. It includes the *Hassan I* dam (built in 1986) and the *Sidi Driss* dam (built in 1984), which ensure the irrigation of agricultural perimeters and the supply of drinking water to the population of the area. The geological formations of the region [AHT Group, 2016] are composed mainly of conglomerates in a band of 2–3 km high aligned at the foot of the *Atlas* that extends northward in the axis of the current course of the *wadi Lakhdar*, and alluvial formations reworked in the quaternary, consisting of pebbles, gravels and sands with high permeability corresponding to former *wadi* beds, and permeable formations pass by going north to silty formations, sometimes encrusted surface. The rest of the northern part of the sub-basin *Lakhdar* is constituted of an alternation of Jurassic (Lias, Jurassic and Jurassic red sandstone of the *High Atlas*). In the southern part, formations of the older secondary (Triassic) and primary outcrop, including the unsubdivided Devonian and the unsubdivided Ordovician.

The studied area is categorized by an arid climate [AHT Group, 2016] with temperate winter covering the entire plain area of the sub-basin (18% of the sub-basin in terms of area), a semi-arid stage with cool winter occupying the piedmont area (12% of the sub-basin), humid with temperate winter covers only 3% of the area of the sub-basin, and humid with cool winter which covers 46% of the area of the sub-basin and most of the mountain area.

Materials

The majority of the data used for this study was gathered from two sources: satellites sources, and rainfall data collected from five ground stations. Satellite data – multispectral images from Landsat satellite sensor, and depending on the date search and image quality used to map land use from the year 2000 to 2020, several types were used: Landsat 7 – Enhanced Thematic Mapper Plus (ETM+), Landsat 5 – Thematic Mapper (TM), Landsat 8 – Operational Land Imager (OLI) sensor images, which were obtained from the U.S. Geological Survey (USGS) (http://earthexplorer. usgs.gov//). All images were acquired during sunny periods, without cloud cover, and were pre-processed (geometric correction with a UTM WGS84 projection and atmospheric correction) in order to compare changes in land cover and land use, all images were acquired at the same period between June and September, which is the period with the stable vegetation stage.

The characteristics of the satellite images and resolution used in this study are summarized in Table 1. Image processing, classification and analysis are performed in ArcGIS 10.3 and ENVI 5.3 software. The processed images have a resolution of about 30 m with multi-spectral bands which facilitates the extraction and characterization of both vegetation cover and bare ground in the study area. The vegetation cover extracted according to these images and according to the field survey, is divided into two main types, forests and cultivated land (arboriculture of different sizes, cereals, olive trees...), and for bare soil it is mainly rocky outcrops bare spaces and / or eroded, and exposed soil (urban areas, rural roads, tracks...). In order to verify and analyze the accuracy of the established maps, precision studies were conducted by determining the confusion matrices, the overly precision and the kappa coefficient [Faruque et al., 2022; Hasan et al. 2020; Kafy et al. 2021].

Meteorological data

The annual and monthly rainfall data made by the hydraulic agency of Oum er-rbia ABHO for the period of 2000 to 2020 were used. The unit of rainfall is the millimeter (mm). The data are

Table 1. Detailed Information of acquired Landsat satellite imagery data used

Landsat	Date (DD/MM/YY)	Resolution (m)	Cloud cover
Landsat 7-ETM+	05 July 2000	30 m	0%
Landsat 5-TM	01July 2007 23 June 2010	30m 30m	0% 0%
Landsat 8-OLI	02 June 2020	30m	0%

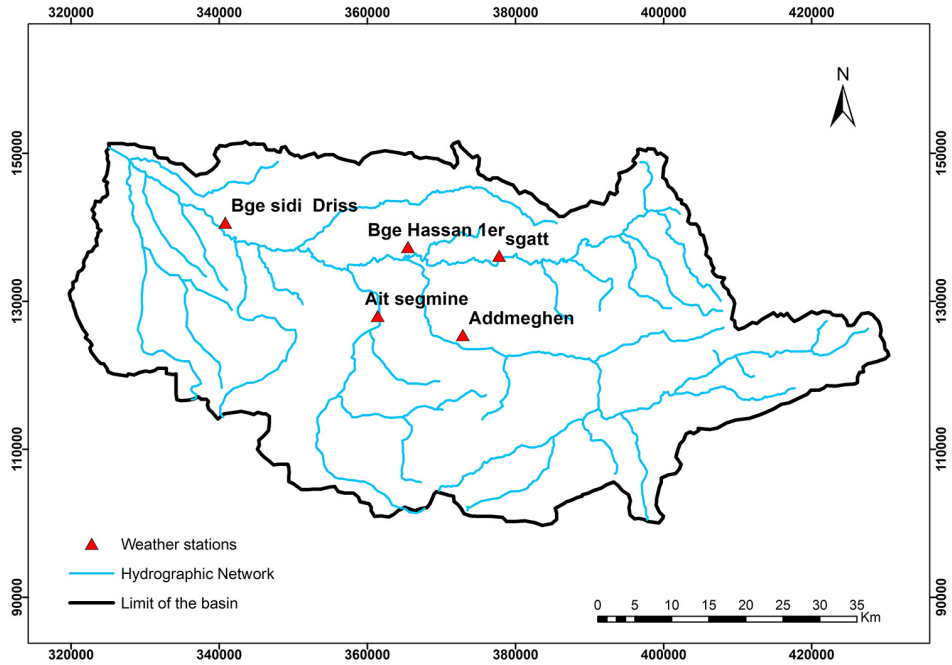

Figure 2. Location of weather stations

organized in a grid. Figure 2 shows the location of the weather stations (5 stations) in the Lakhdar sub-basin district.

Methods

The methodology adopted to study land cover at the different dates and to identify vegetation changes is summarized in Figure 3. The Landsat images used are mainly chosen according to their availability for the study area [Faruque et al. 2022; Hasan et al. 2020]. The downloaded images followed radiometric corrections (Radiometric calibration extension) and atmospheric (semi-automatic extension by the Dark object subtraction model DOS) on ENVI 5.3 software. for the extraction of the study area according to the basin boundaries we used the image mosaic method on Arcgis in order to identify the limits of the area of study.

Image pre-processing

The processing of the images was conducted under ENVI 5.3 software. The images had initialy undergone all geometric and radiometric

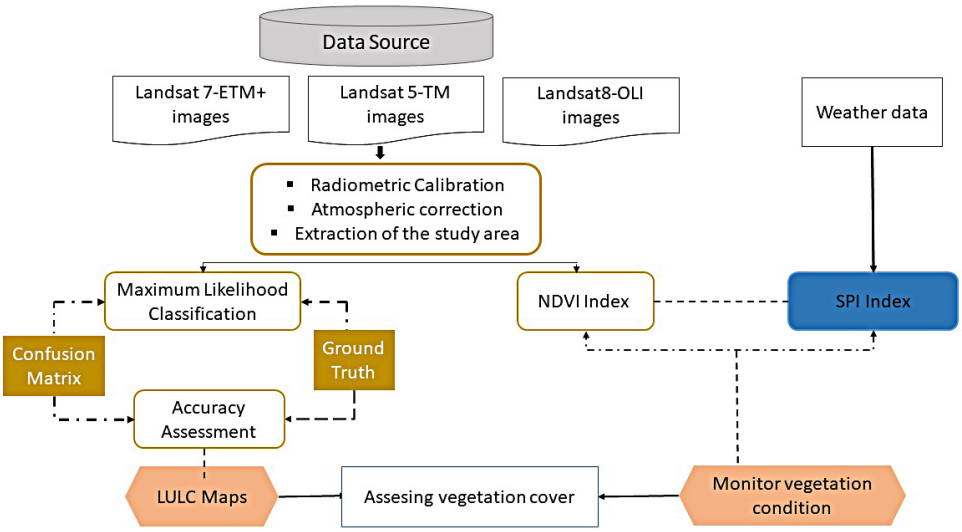

Figure 3. Flowchart of the adopted methodology

corrections in order to correct some variations in the distribution of data due to the time shift during the acquisition of Landsat images Souidi et al., 2020; Vanjare et al., 2014].The radiometric correction aims to correct the scenes acquired according to the properties of the Landsat sensor, it is therefore to impact factors such as the angle of elevation of the sun, the distance earth-sun, the calibration of the sensors, the atmospheric conditions and the geometric sight affecting the numerical value of the pixels [Eckhardt et al., 1990]. While the radiometric corrections applied in this study, consists of converting the raw numerical values (DN) into spectral radiance values under ENVI [Purwanto & al., 2016; Lounis & Aïssa, 2005], by the following equation 1:

$$L_\lambda = (L_{\lambda\max} - L_{\lambda\min})/(DN_{max\lambda} - DN_{min\lambda})* (DN_\lambda - DN_{min\lambda}) + L_{\lambda\min} \quad (1)$$

where: L_λ – spectral radiance at the sensor aperture for a single band mW/(m^2·sr·µm), $L_{\lambda\max}$ and $L_{\lambda\min}$ –scaled spectral radiance (provided in a header file of image information) W/(m^2·sr·µm), DN_{max} – Maximum Digital Number, *DNmin* – minimum digital number.

The images are also influenced by the effects of the atmosphere, hence the need for atmospheric corrections to facilitate the extraction of information from the signal independently of the atmospheric effects that are variable in time and space. The atmospheric correction has been applied by the semi-automatic classification plugin [Chowdhury et al. 2020] based on the Dark Object Subtraction (DOS) algorithm [Congedo, 2020].

Image classification

we used the Arcgis software (GIS) for the supervised classification of the satellite's corrected images [Mohajane et al., 2018; Schroede et al., 2006; Shalaby & Tateishi, 2007]. The principle of this classification using the method of maximum likelihood [Abd El-Kawy et al. 2011; Abebe et al. 2022] is to delimit at the level of the Raster image a set of polygons that will be assigned to a given class of LULC. The method is based on the classification of pixels surrounded by these polygons to create homogeneous spectral signatures, which will present the types of land cover recorded at the image, each class is differentiated from the other according to their characteristics and their spectral response. The training sites obtained will be validated from the visual interpretation of Google Earth images of the study area with the available field surveys.

Based on the field data and using Google Earth high resolution images as reference data, five categories of LULC were identified (Table 2): (1) water body, (2) agriculture, (3) forest, (4) bareland, (5) urban area. These categories were identified and validated using GPS control points and reference data samples to generate training areas of each category.

Accuracy assessment

Accuracy assessment is a very important step in checking the accuracy of the classification results and to identify margin of error caused by the similarity of the spectral response in the distributed classes. The confusion matrix [Acharki et al. 2022; Kumar et al. 2020; Kafy et al. 2021] is the method used to analyze the accuracy in the post-classification phase of LULC images at different dates.

The accuracy study is based on reference data that present the reality of the land cover, and the error evaluation is represented by a confusion or error matrix generated by ENVI 5.3 software. This matrix is in the form of a square table that gathers the pixels of the image where the row represents the classified category [Anand 2012; Jaouda et al. 2018; Purwanto et al. 2016] and the column represents the reality of the field, and the non-diagonal row indicates the values that are misclassified or that are classified in another category. The matrix is also used to calculate the global accuracy,

Table 2. Details of the land use classes

No	Types of land cover class	Color	Color description of classes
1	Water	Blue	River, Canals and Pounds
2	Agriculture	Green	Farmland, crops land and pasture
3	Forest	Green 3	Plants
4	Bareland	Orange	Bare ground
5	Urban	Red	Urban-Inhabited area, Industrial, Mixed build-up Inhabited area, villages and roads

the producer's accuracy, the user's accuracy and the Kappa coefficient [Congalton & Green, 2008; Jazouli et al. 2019; Mohd et al. 2009] The kappa coefficient values are set between 0 and 1, a kappa value higher than 0.80 representing a strong correspondence to reality and a good precision, between 0.4 and 0.8 indicate a medium precision and a value lower than 0.40 indicate a low correspondence between the classification and the real field observation.

NDVI index

Based on Landsat images downloaded in Google Earth and according to the characteristics of the vegetation in the study area and soil type, the NDVI index was mapped to quantify the changes in vegetation over the period (2000–2020).

The NDVI is determined from information on the quantity and density of vegetation by considering the near infrared (NIR) and visible red bands of the electromagnetic spectrum, the index is calculated [Baral et al. 2011; Bijaber et al. 2018; Tadeze et al. 2020], by the following Eq. 2:

$$NDVI = (NIR - RED)/(NIR + RED) \quad (2)$$

where: NIR – represents the reflectance in the near infrared, RED – represents the reflectance in the red band.

NIR and RED represent the radiated reflectance in the near-infrared band 7 (0.8–1.1 μm) and visible red band 5 (0.6–0.7 μm) of the MSS Landsat 5 satellite, respectively. For the TM and ETM+ sensors, the NIR band is band 4, and the RED band is band 3. Finally, for the OLI sensor, the NIR and RED bands are band 5 (0.85–0.88 μm) and band 4 (0.64–0.67 μm) respectively. The NDVI value ranges from -1 to 1. The highest value represents healthy vegetation, while the lowest NDVI value indicates non-vegetation cover.

Reference data was obtained on the area from field surveys and maps published by the hydraulic agency of the study area, and according to extensive discussions with stakeholders, three density classes were determined, namely: The NDVI class with values below 0, presents areas without vegetation cover and according to the reference data they were considered as water bodies and bare soil; the positive values between 0.15 and 0.3 were considered as medium density vegetation (cultivated area); and the positive values above 0.3 were considered as high density vegetation (forest).

SPI Index

SPI is an index developed in 1993 by Mc Kee [Mckee et al. 1995], the determination purpose of this index is to know and monitor drought [Muliawan et al. 2013, Febrina 2017]. According to [Bordi et al. 2011] the SPI method is mainly used because it can give a reliable comparison and is relatively easy to use in various climatic conditions and locations. The rainfall data was provided by ABHO which covers a period of 20 years (2000 to 2020), this data is used to calculate the SPI in R studio software. The SPI is used to measure drought for time scales ranging from 3 months to 28 months. The authors of this index define a drought event when the SPI becomes less than or equal to -1.0 (Table 3). The end of the drought does not occur until the SPI is positive (Edwards et al., 1997). The Standardized Precipitation Index has the following Equation 3:

$$SPI = \frac{P - Pm}{\sigma p} \quad (3)$$

where: P – total rainfall of a period (mm), Pm – historical average rainfall of the period (mm), σp – historical standard deviation of rainfall for the period (mm).

This index defines the severity of drought in different classes (Table 3) [OMM, 2012]. Negative annual values indicate a drought compared to the chosen reference period and positive values indicate a wet period. The SPI allows us to measure drought at different time scales that range from 3 months to 28 months (Table 4) [OMM, 2012]., these indices offer temporal flexibility in assessing rainfall conditions in relation to water supply.

Table 3. SPI index classes

SPI classes	Degree of drought
SPI >2	Exceptional wet
1<SPI<2	Severe wet condition
0<SPI<1	Medium wet condition
-1<SPI<0	Slight drought
-2<SPI<-1	Severe dought
SPI<-2	Exceptional drought

RESULTS

Land uses/land cover changes monitoring LULC

The LULC classification map were conducted using Landsat multi-date images from the years

Table 4. SPI index application

Duration SPI	Reflected incidents	Application
SPI 1 month	Short-term conditions	Short-term soil moisture and crop stress (especially during the growing season).
SPI 3 months	Short and medium term humidity conditions	A seasonal estimate of precipitation
SPI6 months	Medium-term precipitation trends SPI	Ability to effectively show precipitation over separate sessions. For example, for California, the 6-month SPI can effectively show the amount of precipitation from October to March.
SPI9 months	Precipitation motifs on a medium time scale	If SPI 9 < -1.5 then this is a good indication that substantial impacts may occur in agriculture (as well as the possibility of other sectors).
SPI12 months	Forms of long-term precipitation	Possible flows related to reservoir levels, and also groundwater levels.

Table 5. Land-cover (in hectare and percentage) from 2000 to 2020

LULC classes	2000		2007		2010		2020	
	Area (ha)	%	Area (ha)	%	Area (ha)	%	Area (ha)	%
Agriculture	40798.66	11.21%	8809.60	2.42%	17232.32	4.74%	15751.47	4.33%
Forest	22818.38	6.27%	28478.18	7.83%	23312.42	6.41%	27312.89	7.51%
Bareland	297802.69	81.86%	323316.99	88.87%	318541.28	87.56%	315055.49	86.60%
Urban	97.31	0.03%	977.56	0.27%	980.63	0.27%	2988.26	0.82%
Water	2296.74	0.63%	2233.28	0.61%	3747.25	1.03%	2704.39	0.74%
Total	363813.78	100%	363815.62	100%	363813.91	100%	363812.51	100%

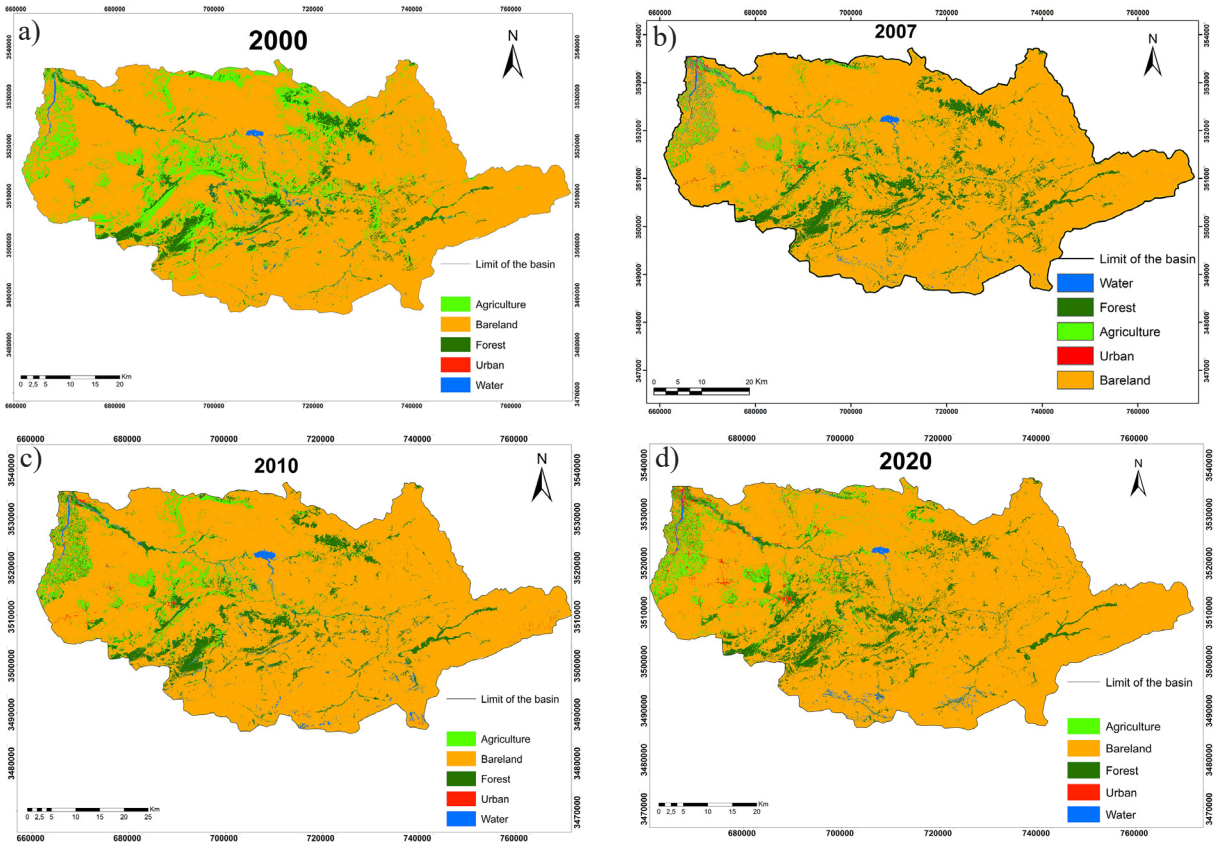

Figure 4. LULC maps for the years (a) 2000, (b) 2007, (c) 2010, and (d) 2020 in the studied area

2000 to 2020 by the ML maximum likelihood method, as shown in Figure 4. The results of this classification (Table 5 and Figure 4), show very significant changes in terms of vegetation cover, urban area, and bare soil. The most remarkable changes were noticed in terms of vegetation cover

(agricultural and forest area) and urban area, vegetation area decreased from 63,617 ha (17%) in 2000 to 43,064 ha (12%) in 2020, while the bare soil increased by 5% going from 297,802 ha (82%) in 2000 to 315,055 ha (87%) in 2020, the urban area also increased from 97.31 ha (0.03%) in 2000 to 2988.26 ha (0.87%) in 2020, finally, the water body has remained more or less stable by 2296.74 ha (0.63%) in 2000 to 2704.39 ha (0.74%) in 2020.

Accuracy assessment

The accuracy assessment using the confusion matrix in the post classification phase. The results of this classification give values of Overly Accuracy of the order: 90%, 79%,82%,93% for the years 2000, 2007, 2010, 2020 respectively and a kappa coefficient of 0.8473, 0.7091, 0.7492, 0.8814 respectively (Table 6). The Kappa coefficient [Anand, 2012; Baral et al. 2011; Xie & Ren, 2011] is a statistical measurement technique of the gap between the reference value (real image) and the identified classification value (classified image), the acceptable values which present a good correspondence between the classified pixels and the reference pixels set between 0.61 and 1 [Anand, 2012; Baral et al., 2011], the blue cells of

Table 6. Accuracy assessment of the land cover maps generated (2000–2020)

Year 2000							
Classes	Water	Agriculture	Forest	Urban	Bareland	Producer's accuracy	User's accuracy
Water	1093	29	11	12	135	75.07%	85.39%
Agriculture	119	920	47	11	197	91.82%	71.10%
Forest	37	16	1053	0	7	94.44%	94.61%
Urban	127	16	2	270	21	91.53%	61.93%
Bareland	80	21	2	2	4766	92.98%	97.84%
Overall Accuracy = (8196/9088) 90.1849%							
Kappa Coefficient = 0.8473							
Year 2007							
Classes	Vegetation	Water	Bareland	Urban		Producer's accuracy	User's accuracy
Vegetation	1958	10	137	22		89.04%	92.05%
Water	42	368	133	5		91.32%	67.15%
Bareland	92	12	1480	166		68.90%	84.57%
Urban	107	13	398	321		62.45%	38.26%
Overall Accuracy = (4422/5559) 79.5467%							
Kappa Coefficient = 0.7091							
Year 2010							
Classes	Water	Forest	Agriculture	Bareland	Urban	Producer's accuracy	User's accuracy
Water	1737	25	3	280	58	76.05%	82.60%
Forest	96	3435	8	58	9	88.14%	95.26%
Agriculture	46	337	323	24	52	94.17%	41.30%
Bareland	171	43	0	6191	142	80.64%	94.56%
Urban	234	51	9	1124	1055	80.17%	42.66%
Overall Accuracy = (12922/15698) 82.3162%							
Kappa Coefficient = 0.7492							
Year 2020							
Classes	Water	Bareland	Agriculture	Forest	Urban	Producer's accuracy	User's accuracy
Water	113	18	0	0	20	83.70%	74.83%
Bareland	3	1431	0	2	5	92.38%	99.31%
Agriculture	0	4	131	12	3	97.04%	87.33%
Forest	1	0	0	236	0	94.40%	99.58%
Urban	18	96	4	0	243	89.67%	67.31%
Overall Accuracy = (2355/2541) 92.6800%							
Kappa Coefficient = 0.8814							

the matrix (diagonal) present the acceptable classified pixels between the reference image and the classified image. The user and producer accuracies of the classes for the period under study are presented in Table 6, and the results obtained indicate that almost all the classes present user and producer accuracy values higher than 80% proving a good accuracy of the classification method.

Spatial distribution of NDVI over 2000 to 2020

The NDVI measures the balance between the energy received and emitted by ground objects and thus characterizes the vegetation mass present in a given environment [Rouse et al., 1973]. In principle, positive values correspond to denser vegetation and negative values to bare ground, clouds, lakes and rivers. In this study the NDVI is determined based on satellite images taken in the same period of the year (June & July). The values obtained vary from -0.55 to 0.75 over a period of 20 years (Figure 5). According to the results obtained (Figure 5), each map shows variations in NDVI values for the study area. NDVI varies from a positive value of 0 (very low to no photosynthetic activity) to 0.77 (very

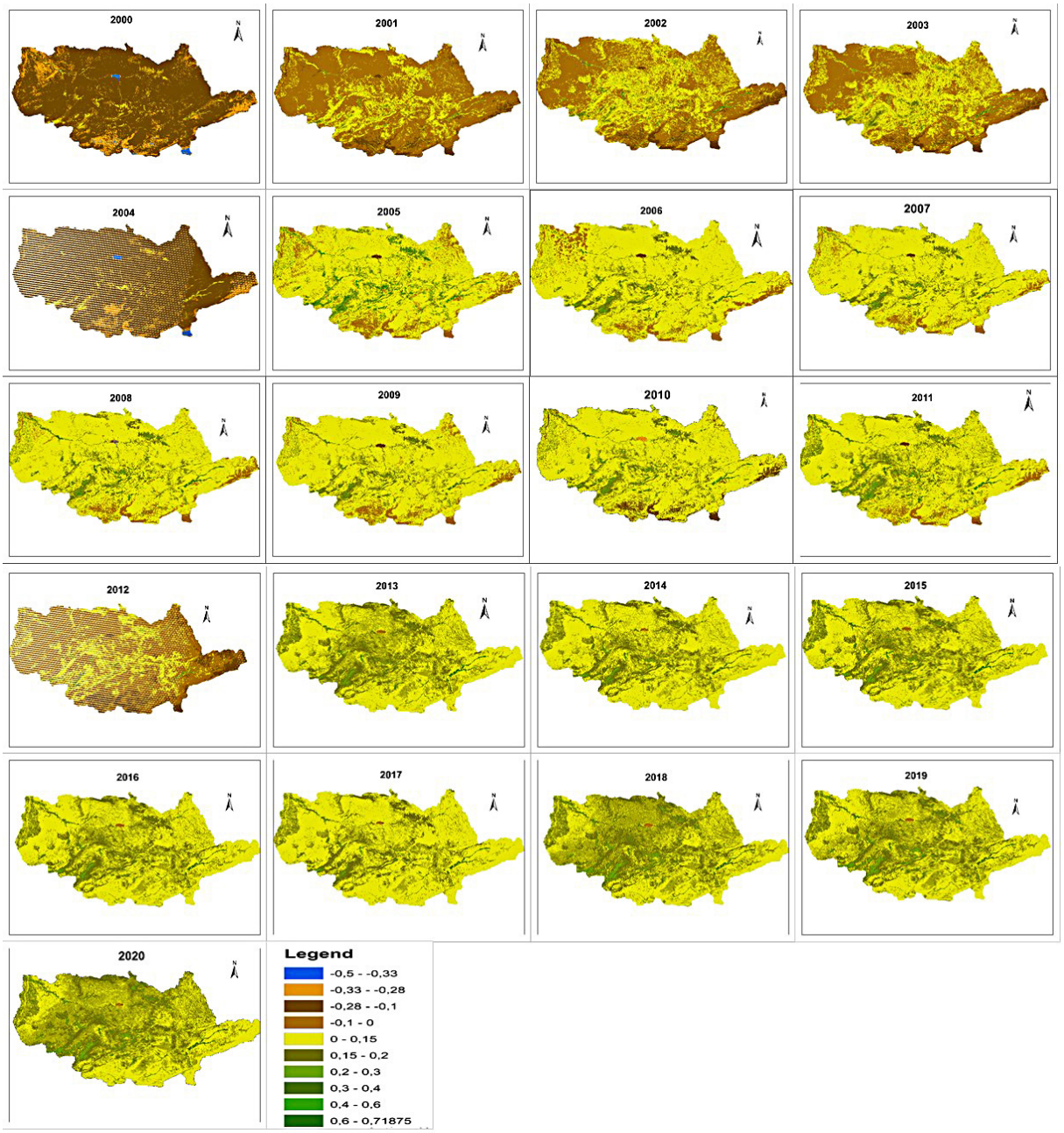

Figure 5. NDVI cover changes maps 2000 to 2020

Figure 6. SPI Index 2000 to 2020

heavy and dense vegetation). The values between 0.15 and -0.28 are often assimilated to bare soil, while the very negative values below -0.28 present other forms of land use, they are attributed in this case and according to field surveys to water bodies or snow. In terms of variation over time, the state of vegetation has undergone very significant changes from one year to another, where we can see from Figure 5 that the lowest values are observed during the period 2000 to 2004 (drier period) with indices of -0.55 to 0.58. On the other hand, the highest values, which present a more important vegetation activity, are detected from the year 2013 to 2020 (wetter period) with indices that vary between -0.20 to 0.75. For the rest of the time series the values present globally average indices of photosynthetic activity.

SPI Index

Being standardized, the SPI has the advantage of comparing drought conditions over various time periods. The values of SPI are calculated using R studio software. Comparison of the 3-months, 6-months and 9-months seasonal SPI indices highlights the seasonal characteristics of rainfall and drought conditions. Figure 6 shows that during 2018–2020, the summer season SPI3 was particularly negative with values reaching -2.8. The variation of SPI6 shows negative values that do not exceed -1 in 2001 and 2008. For SPI 9 and SPI12 it shows the same variation trend. SPI12 presents annual variations and highlights an alternation of dry and wet years during the periods from 2000 to 2002 and from 2008 to 2009, where the SPI values reach -1 resulting in strong drought, on the other hand the wet periods are from 2004 to 2005 and from 2012 to 2015 which has positive values of the order of 1.

DISCUSSION

LULC changes from 2000 to 2020

The analysis of land change (Table 5 and Figure 5) shows an increase in the urban area from 0.03% to 0.83% between 2000 and 2020 caused by the population density increase and a remarkable decrease in vegetation, mainly explained by the climate change impact causing frequent dry seasons. Among the strategies adopted for this area by the Hydraulic Agency of Oum-Erbia, building several dams to collect surface water aiming to improve the sustainability of these resources. That improvement is clearly noticeable in our mapping according to Table 3 and Figure 5, a significant increase in water resources from 0.63% in 2000 to 1.03% in 2010, which generate an increase in the vegetation area that can be seen in Table 3 (jumping from 10.25% in 2007 to 11.14% in 2010). Unfortunately, from 2010 other constraints cause the considerable decrease in these resources such as the accentuated impact of dry seasons and the important decrease of precipitation which result into a decrease of water cover from 1.03% in 2010 to 0.74% in 2020.The overall accuracy and Kappa coefficients for the LULC maps from 2000 to 2020 shows a good accuracy, which proves that the Maximum Likelihood Supervised Classification method used in this study was very effective in improving the land use classification. The conditional Kappa statistics of each LULC class were all between 0.70 to 0.80, except for barren land. Barren land can be confused with urban areas where the accuracy of the producer and user (Table 4) does not exceed 60%, this limitation of the obtained accuracy values is mainly due to the rather similar reflectance effect between the two categories.

Similarly Chooi et al. [2010], studied the urbanization and the resulting land use change by analyzing Landsat satellite images during the period from 1999 to 2007 in Penang Island, Malaysia, they chosed the maximum likelihood classification method, their study reveal that the urban area increased dramatically, and the grassland area increased moderately. Conversely, barren land decreased obviously, and forest area decreased moderately. They found according to their study that the maximum likelihood classification produced superior results and achieved a high degree of accuracy and that The remote sensing technique used in their study proved to be effective; it reduced the analysis time of urban expansion and proved to be a useful tool for assessing the impact of urbanization on LST. Ozesmi & Bauer, [2002] confirmed that the MLC leads to higher accuracy than the decision tree (DT) classification. In a related investigation at the same profile region, remote sensing geospatial technologies have been used with great effectiveness. For instance, based on the supervised classification algorithm and the normalized difference vegetation index NDVI, Barakat et al. [2018] used Sentinel-2A MSI images and ASTER (Advanced

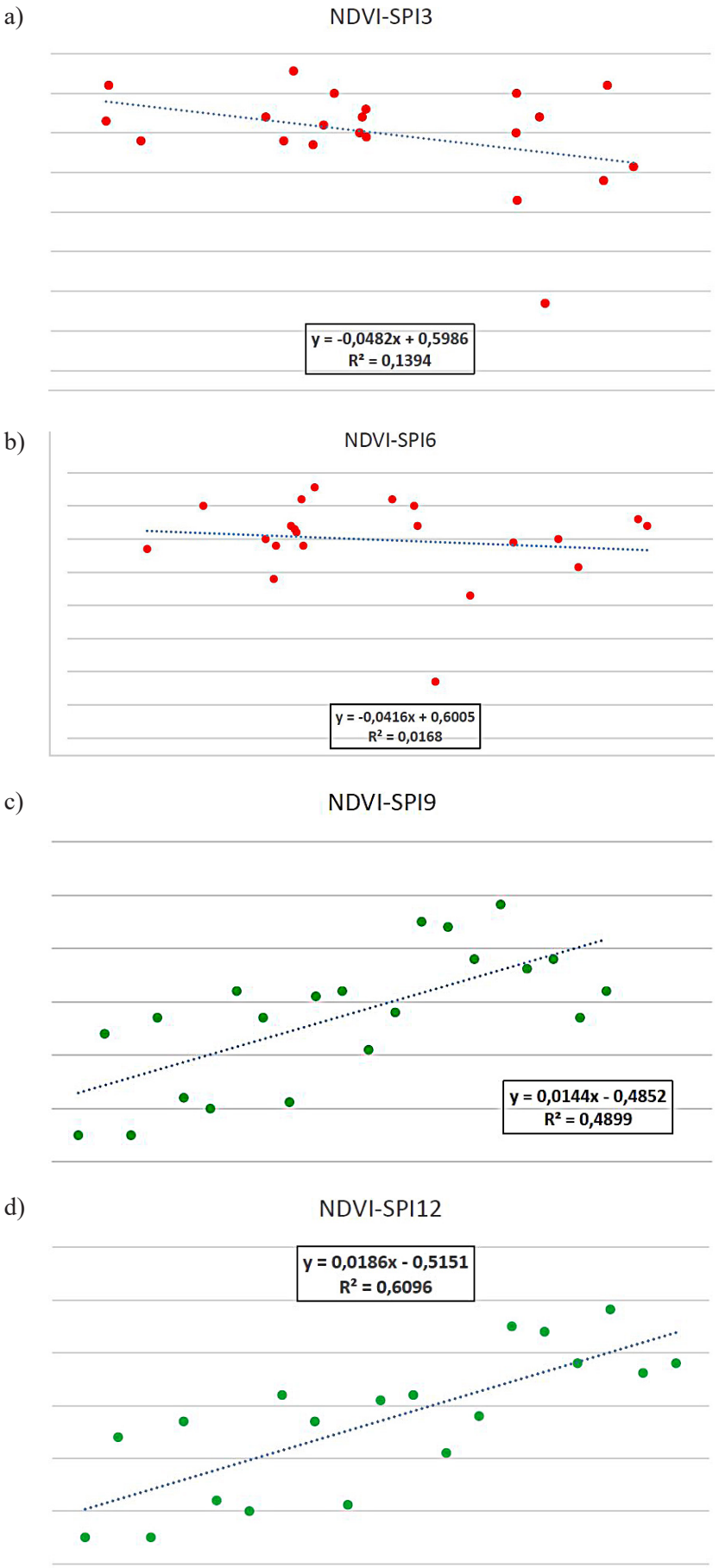

Figure 7. Correlation between SPI Index and NDVI

Spaceborne Thermal Emission and Reflection Radiometer) images acquired from 2001 to 2015 to quantify changes in the Eastern area of Béni-Mellal province. According to their report, the amount of forest land has increased as a result of changes in land use. Haboudane & Bahri [2007] employed spectral mixture analysis (SMA) and maximum likelihood classification (MLC) to map multidate satellite images from Thermic Mapper (TM), Enhanced Thermic Mapper Plus (ETM+), and Advanced Spaceborne Thermal Emission and Reflection Radiometer (ASTER).

Vegetation monitoring NDVI and SPI indexes

The revelation of a relationship between NDVI and SPI was tested by calculating correlation coefficients "r" according to a multiple regression model and the coefficient of determination "R^2" between the different variables. The scattering of points on the SPI3/NDVI and SPI6/NDVI scatterplot illustrates a weak correlation between these two indices (Figure 7). The coefficients of determination R^2 between NDVI and SPI vary according to the time scale considered, which means that NDVI is not significantly correlated with SPI3 and SPI6 which show seasonal variations. On the other hand, we can notice a slightly significant correlation with SPI9, which has an R^2 of about 0.489, and it is more correlated with SPI12 where we have an R^2 of 0.61 (Figure 7).

Similar studies have been conducted, by Lei & Peters [2004] who confirms that the response of vegetation to precipitation is with a time lag, and the impact of water deficits on vegetation is cumulative. Rokhmatullah et al. [2019] studied the problem of dryness that occurs in several regions in Indonesia (Bekasi), where they monitored this phenomenon by using SPI and NDVI index to find the relationship between these two, the result of this research shows that there is a close relationship between a region with high NDVI value and SPI value. But in a region with a low NDVI value, several regions have high SPI values.

CONCLUSIONS

The objective of our study was to determine the LULC status over the entire period from 2000 to 2020, to characterize the vegetation cover that will influence the land erosion at *Lakhdar* sub-basin in Morocco. Thanks to processing and analyzing remote sensing and satellite images under computer tools (ENVI software and GIS), and field surveys a detailed study was conducted on the occupation and use of land in the area. The use of multi-date images and different satellites and sensors allowed to update the LULC over a period of 20 years.

During the 20-year period, several changes are observed in the *Lakhdar* sub-basin. The results of the supervised classification by the method of maximum likelihood, can be summarized as follows: a significant decrease in the vegetation cover of (5%), and a considerable increase in the bare land and urban environment during this period. This classification accuracy is checked using a confusion matrix to determine the margin of error between the classified images and the reference images with control points based on the field survey.

The accuracy values obtained show high values for all images where the value of OA shows a good classification and presentation of reality. The obtained results of accuracy using the value of OA and Kappa coefficient, prove that the supervised classification by the method of maximum likelihood is an effective method to identify the changes of LULC and it is also a strong tool in decision making to have a better management and preservation of this basin. The results of correlation between the point index based on climatic data (SPI) and the spatial index based on satellite images (NDVI), gave limited correlations with seasonal variations (SPI3 and SPI6), and a more significant correlation with the annual and average variation (SPI9 and SPI12). To characterize and monitor the state of vegetation, the SPI remains very limited in these applications, as it is based on defined locations data from weather stations and therefore does not present the spatial impact on the entire area, and it is an index that is calculated based on only rainfall data, and it neglects the influence of other phenomenon on the water status of the area, such as evaporation and temperature. On the other hand, the NDVI gives a better modeling of vegetation status and with more accuracy on the areas affected by drought. It is an index based on the use of satellite images, which allows a better mapping of daily luminance levels and it also clarified the inter and intra-annual variations of the greens which can be influenced by climatic conditions. The advantage of this approach is providing an impact analysis of the different spatial and climatic components on the state of vegetation, moving from the location scale SPI to the regional scale NDVI while keeping the same scientific rigor.

REFERENCES

1. Abd El-Kawy, O.R., Rød, J.K., Ismail, H.A., Suliman, A.S. 2011. Land use and land cover change detection in the western Nile delta of Egypt using remote sensing data. Applied Geography, 31(2), 483–494. https://doi.org/10.1016/j.apgeog.2010.10.012
2. Abebe, G., Getachew, D., Ewunetu, A. 2022. Analysing land use/land cover changes and its dynamics using remote sensing and GIS in Gubalafito district, Northeastern Ethiopia. SN Applied Sciences, 4(1). https://doi.org/10.1007/s42452-021-04915-8
3. Acharki, S., El Qorchi, F., Arjdal, Y., Amharref, M., Bernoussi, A.S., Ben Aissa, H. 2022. Soil erosion assessment in Northwestern Morocco. Remote Sensing Applications: Society and Environment, 25, 100663.
4. Anand, A. 2012. Unit 14 Accuracy Assessment. Processing and Classification of Remotely Sensed Images, January 2017, 59–77. https://www.researchgate.net/publication/319963167_processing_and_classification_of_remotely_sensed_images
5. AHT Group, F., Ag, A.H.T.G., Avril, R. 2016. Diagnostic du sous-bassin de Lakhdar.
6. Lounis, B., Aïssa, A.B. 2005. Processus de Correction Radiométrique Relative «PCRR» Appliqué Aux Images Landsat TM Multi- Dates. 3rd International Conference: Sciences of Electronic, Technologies of Information and Telecommunications, 1–7.
7. Barakat, A., Khellouk, R., El Jazouli, A., Touhami, F., Nadem, S. 2018. Monitoring of forest cover dynamics in eastern area of Béni-Mellal Province using ASTER and Sentinel-2A multispectral data. Geology, Ecology, and Landscapes, 2(3), 203–215. https://doi.org/10.1080/24749508.2018.1452478
8. Baral, G.P., Mcdougall, K., Chong, A. 2011. Review of Australian Land Use Mapping and Land Management Practice. 21, 199–210.
9. Bahri, E.M. 2007. Essai de cartographie des espèces forestières dominantes dans le Moyen Atlas (Maroc) à partir des données ASTER To cite this version : HAL Id : hal-01946833. January.
10. Bijaber, N., Hadani, D., El, Saidi, M., Svoboda, M.D., Wardlow, B.D., Hain, C.R., Poulsen, C.C., Yessef, M., Rochdi, A. 2018. Developing a Remotely Sensed Drought Monitoring Indicator for Morocco. https://doi.org/10.3390/geosciences8020055
11. Bordi, I., Fraedrich, K., Sutera, A. 2009. Observed drought and wetness trends in Europe: An update. Hydrology and Earth System Sciences, 13(8), 1519–1530. https://doi.org/10.5194/hess-13-1519-2009
12. Chowdhury, M., Hasan, M.E., Abdullah-Al-Mamun, M.M. 2020. Land use/land cover change assessment of Halda watershed using remote sensing and GIS. Egyptian Journal of Remote Sensing and Space Science, 23(1), 63–75. https://doi.org/10.1016/j.ejrs.2018.11.003
13. Congedo, L. 2020. Semi-Automatic Classification Plugin Documentation Release 7.9.5.1. User Manual, August, 1–225.
14. Chavez, P.S., Jr. 1988. An improved dark-object subtraction technique for atmospheric scattering correction of multispectral data. Remote Sens. Environ., 24, 459–479.
15. Dodamani, B.M., Anoop, R., Mahajan, D.R. 2015. Agricultural Drought Modeling Using Remote Sensing. International Journal of Environmental Science and Development, 6(4), 326–331. https://doi.org/10.7763/ijesd.2015.v6.612
16. Faruque, M.J., Hasan, M.Y., Islam, K.Z., Young, B., Ahmed, M.T., Monir, M.U., Shovon, S. M., Kakon, J.F., Kundu, P. 2022. Monitoring of land use and land cover changes by using remote sensing and GIS techniques at human-induced mangrove forests areas in Bangladesh. Remote Sensing Applications: Society and Environment, 25(July 2021), 100699. https://doi.org/10.1016/j.rsase.2022.100699
17. Haboudane, D. 2007. Deforestation detection and monitoring in cedar forests of the Moroccan Middle-Atlas Mountains. In Proceedings of the 2007 IEEE International Geoscience and Remote Sensing Symposium, Barcelona, Spain 2007, 4327–4330
18. Hasan, S., Shi, W., Zhu, X., Abbas, S., Khan, H.U.A. 2020. Future simulation of land use changes in rapidly urbanizing South China based on land change modeler and remote sensing data. Sustainability (Switzerland), 12(11), 4–6. https://doi.org/10.3390/su12114350
19. Gurgel, R.S., Farias, P.R.S., De Oliveira, S.N. 2017. Land use and land cover mapping and identification of misuse in the permanent preservation areas in the Tailândia Municipality - PA. Semina: Ciencias Agrarias, 38(3), 1145–1160. https://doi.org/10.5433/1679-0359.2017v38n3p1145
20. Hasan, S., Shi, W., Zhu, X., Abbas, S., Khan, H.U.A. 2020. Future simulation of land use changes in rapidly urbanizing South China based on land change modeler and remote sensing data. Sustainability (Switzerland), 12(11), 4–6. https://doi.org/10.3390/su12114350
21. Maina J., Wandiga S., Gyampoh B. Charles K.K.G. 2020. Assessment of Land Use and Land Cover Change Using GIS and Remote Sensing: A Case Study of Kieni, Central Kenya. Journal of Remote Sensing & GIS, 9(1), 1–5. https://doi.org/10.35248/2469-4134.20.9.270
22. Jaouda, I., Akhssas, A., Ouadif, L., Bahi, L., Lahmili, A. 2018. Stabilite des talus et impact sur le reseau routier: cas du bassin versant d'Ouergha (Maroc). MATEC Web of Conferences, 149. https://doi.org/10.1051/matecconf/201714902052
23. Jazouli, A., El Barakat, A., Khellouk, R., Rais, J., Baghdadi, M.E. 2019. Remote sensing and GIS techniques for prediction of land use land cover change

effects on soil erosion in the high basin of the Oum Er Rbia River (Morocco). Remote Sensing Applications: Society and Environment, 13 (Dec. 2018), 361–374. https://doi.org/10.1016/j.rsase.2018.12.004

24. Jiang, J., Tian, G. 2010. Analysis of the impact of Land use/Land cover change on Land Surface Temperature with Remote Sensing. Procedia Environmental Sciences, 2(5), 571–575. https://doi.org/10.1016/j.proenv.2010.10.062
25. Ji, L., Peters, A.J. 2004. Forecasting Vegetation Greenness With Satellite and Climate Data. IEEE Geoscience and Remote Sensing Letters, 1(1), 3–6. https://doi.org/10.1109/LGRS.2003.821264
26. Kumar, S., Shwetank, Jain, K. 2020. A multi-temporal landsat data analysis for land-use/land-cover change in haridwar region using remote sensing techniques. Procedia Computer Science, 171, 1184–1193.
27. Kafy, A.A, Faisal, A.A., Shuvo, R.M., Naim, M.N.H., Sikdar, M.S., Chowdhury, R.R., Islam, M.A., Sarker, M.H.S., Khan, M.H.H., Kona, M.A. 2021. Remote sensing approach to simulate the land use/land cover and seasonal land surface temperature change using machine learning algorithms in a fastest-growing megacity of Bangladesh. Remote Sensing Applications: Society and Environment, 21 (Dec. 2020), 100463. https://doi.org/10.1016/j.rsase.2020.100463
28. Mohajane, M., Essahlaoui, A., Oudija, F., Hafyani, M., El, Hmaidi, A., El, Ouali, A., El, Randazzo, G., Teodoro, A.C. 2018. Land use/land cover (LULC) using landsat data series (MSS, TM, ETM+ and OLI) in azrou forest, in the central middle atlas of Morocco. Environments - MDPI, 5(12), 1–16. https://doi.org/10.3390/environments5120131
29. Mohd Hasmadi, I., Pakhriazad, H.Z., Shahrin, M.F. 2009. Evaluating supervised and unsupervised techniques for land cover mapping using remote sensing data. Malaysiann Journal of Society and Space, 5(1), 1–10.
30. Onuche, N.C. (n.d.). Remote sensing and gis based application for land use mapping and urban renewal in Hayin Dogo, Samaru By.
31. Organisation Météorologique Mondiale. 2012. Guide d'utilisation de l'indice de précipitations normalisé. Temps. Climat. Eau, 1090, 17. http://www.droughtmanagement.info/literature/WMO_standardized_precipitation_index_user_guide_fr_2012.pdf
32. Ozesmi, S.L., Bauer, M.E. 2002. Satellite Remote Sensing of Wetlands. Wetland Ecology and Management, 10, 381-402. http://dx.doi.org/10.1023/A:1020908432489
33. Pang, C., Yu, H., He, J., Xu, J. 2013. Deforestation and changes in landscape patterns from 1979 to 2006 in Suan County, DPR Korea. Forests, 4, 968–983.
34. Purwanto, Utomo, D.H., Kurniawan, B.R. 2016. Spatio Temporal Analysis Trend of Land Use and Land Cover Change Against Temperature Based on Remote Sensing Data in Malang City. Procedia - Social and Behavioral Sciences, 227, 232–238. https://doi.org/10.1016/j.sbspro.2016.06.066
35. Rasool, R., Fayaz, A., Shafiq, M.U, Singh, H., Ahmed, P. 2021. Land use land cover change in Kashmir Himalaya: Linking remote sensing with an indicator based DPSIR approach. Ecological Indicators, 125, 107447. https://doi.org/10.1016/j.ecolind.2021.107447
36. Rokhmatullah, Hernina, R., Yandi, S. 2019. Drounght Analysis by Using Standarized Precipitation Index (SPI) and Normalized Difference Vegetation Index (NDVI) at Bekasi Regency in 2018. IOP Conference Series: Earth and Environmental Science, 280(1). https://doi.org/10.1088/1755-1315/280/1/012002
37. Shalaby, A., Tateishi, R. 2007. Remote sensing and GIS for mapping and monitoring land cover and land-use changes in the Northwestern coastal zone of Egypt. Applied Geography, 27(1), 28–41. https://doi.org/10.1016/j.apgeog.2006.09.004
38. Souidi, H., Ouadif, L., Bahi, L., Elhachmi, D., Edderkaoui, R. 2020. Application of stochastic process & cellular automata integrated to GIS for land monitoring: Coastal Chaouia, Morocco. International Journal of Advanced Research in Engineering and Technology, 11(5), 245–252. https://doi.org/10.34218/IJARET.11.5.2020.026
39. Tadese, M., Kumar, L., Koech, R., Kogo, B.K. 2020. Mapping of land-use/land-cover changes and its dynamics in Awash River Basin using remote sensing and GIS. Remote Sensing Applications: Society and Environment, 19, 100352. https://doi.org/10.1016/j.rsase.2020.100352
40. Tan, K.C., Lim, H.S., MatJafri, M.Z., Abdullah, K. 2010. Landsat data to evaluate urban expansion and determine land use/land cover changes in Penang Island, Malaysia. Environmental Earth Sciences, 60(7), 1509–1521. https://doi.org/10.1007/s12665-009-0286
41. Vanjare, A., Omkar, S.N., Senthilnath, J. 2014. Satellite Image Processing for Land Use and Land Cover Mapping. International Journal of Image, Graphics and Signal Processing, 6(10), 18–28. https://doi.org/10.5815/ijigsp.2014.10.03
42. Xie, F., Lin, Y., Ren, W. 2011. Optimizing model for land use/land cover retrieval from remote sensing imagery based on variable precision rough sets. Ecological Modelling, 222(2), 232–240. https://doi.org/10.1016/j.ecolmodel.2010.08.011